Stable second-order scheme for integrating the Kuramoto-Sivanshinsky equation in polar coordinates using distributed approximating functionals

Peter Blomgren,* Scott Gasner,† and Antonio Palacios‡
Nonlinear Dynamical Systems Group, Department of Mathematics and Statistics, San Diego State University, San Diego, California 92182, USA
(Received 13 December 2004; published 6 September 2005)

We present an algorithm for the time integration of nonlinear partial differential equations. The algorithm uses distributed approximating functionals, which are based on an analytic approximation method, in order to achieve highly accurate spatial derivatives. The time integration is based on a second-order unconditionally *A*-stable Crank-Nicolson scheme with a Newton solver. We apply the integration scheme to the Kuramoto-Sivanshinsky equation in polar coordinates, which presents a significant computational challenge due to the stiffness introduced by the estimation of the spatial derivatives at the origin. We present several stationary and nonstationary solutions of the Kuramoto-Sivanshinsky equation and compare with previous numerical results as well as patterns observed in the combustion front of a circular burner. The numerical results of the proposed scheme reproduces several patterns—rotating two-cell, three-cell, hopping three-cell, stationary two-three- four- and five-cell, stationary 5/1,6/1,7/1,8/2 two-ring patterns, etc.—observed in physical experiments. The scheme is extremely robust and can produce long-term simulations consisting of several thousand frames. Although applied to a very specific problem, the approach of combining the framework of distributed approximating functionals with a Crank-Nicolson based time integration is generalizable to a large class of problems.

DOI: 10.1103/PhysRevE.72.036701 PACS number(s): 02.60.Cb, 02.70.−c, 05.45.−a, 47.54.+r

I. INTRODUCTION

Pattern formation governed by complex spatiotemporal dynamics is of great interest and has been studied in many applications, e.g., chemical systems [1], fluid convection [2], flame-front propagation [3–6], etc. The qualitative behavior of the pattern formation can be studied using simplified models; in the case of cellular flames stabilized on a circular porous plug burner the Kuramoto-Sivashinsky equation [7–9] is one example of a simplified model.

The motivation for the study of the wide array of complex cellular flame patterns formed on a circular plug burner is to increase the understanding of, and be able to suppress cellular flame instability associated with dynamic patterns in order to design an efficient burner system. Extended experimental studies in which several complex states have been categorized have been performed [4–6,10]. The uniform flame front can undergo symmetry-breaking bifurcations and produce interesting stationary and nonstationary or dynamic multicell patterns.

The present paper is an extension of [11] which proposes a scheme for the time integration of the Kuramoto-Sivanshinsky equation. The scheme proposed here is second-order accurate in time. Further, this scheme, in which the time integration is based on the Crank-Nicolson method [12], is unconditionally *A*-stable (see the Appendix), thus producing finite solutions in all cases where theexact solution of the underlying equation produces finite solutions.

The favorable stability property of the proposed scheme allows us to produce long-term simulations consisting of several thousands of frames in the time evolution of the Kuramoto-Sivanshinsky equation, which expressed in polar coordinates can be written as

$$u_t = -u_{rrrr} - \frac{1}{r^4}u_{\phi\phi\phi\phi} - \frac{2}{r^2}u_{rr\phi\phi} - \frac{2}{r}u_{rrr} + \frac{2}{r^3}u_{r\phi\phi} - \left(2 - \frac{1}{r^2}\right)u_{rr} - \left(\frac{4}{r^4} + \frac{2}{r^2}\right)u_{\phi\phi} - \left(\frac{1}{r^3} + \frac{2}{r}\right)u_r + \eta_1 u - \eta_2\left(u_r^2 + \frac{1}{r^2}u_\phi^2\right) - \eta_3 u^3. \quad (1)$$

The unconditionally *A*-stable Crank-Nicolson scheme employed with an iterative Newton solver to resolve the resulting nonlinear system of equations is an appropriate scheme as it is an accurate method which allows much larger time steps than simpler linearizion schemes, based on, e.g., a fixed-point solver applied to the same system of nonlinear equations, or the linearization scheme proposed in [11].

We note that this approach of basing the time integration of a complex system on using the framework of distributed approximating functionals to generate highly accurate numerical representation of the derivatives, combined with an implicit Crank-Nicolson based time integration with excellent stability properties, is quite general. The methodology described in the present paper is highly generalizable to other problems expressed in the form of a time-dependent partial differential equation on a regular or nonregular grid.

II. NUMERICAL CHALLENGES

Numerical investigation of cellular flames in a circular burner using the Kuramoto-Sivanshinsky equation (1) has

*Electronic address: blomgren@mail.SDSU.EDU; URL: http://terminus.sdsu.edu/
†Electronic address: sgasner@yahoo.com
‡Electronic address: palacios@euler.SDSU.EDU

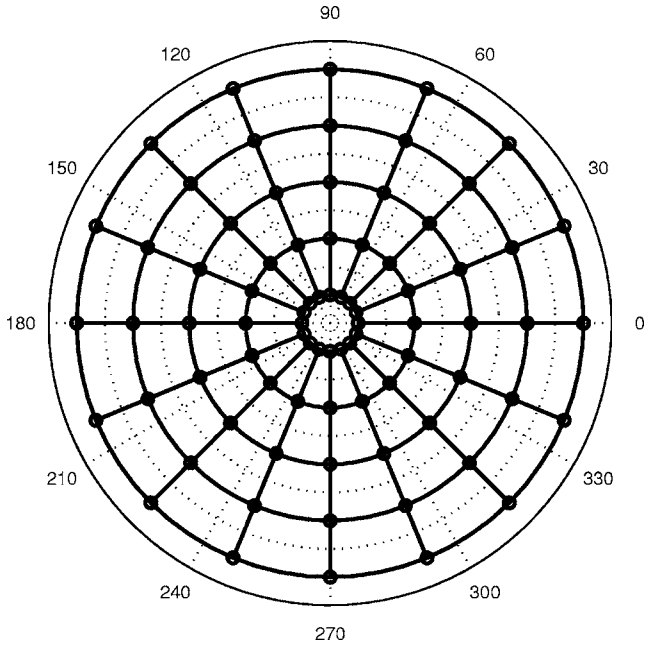

FIG. 1. The polar grid. Notice that the innermost points are located at a radius $r=dr/2$; hence there is no computational point at the center of the grid. The radial spacing is dr. In our computations we use 32 radial points and 64 azimuthal points, i.e., $dr=R/32.5$ and $d\phi=2\pi/64$.

been elusive due to the singularity that arises in the biharmonic operator $\nabla^4=[\partial_{rr}+2(1/r)\partial_r+(1/r^2)\partial_{\phi\,\phi}]^2$, near the origin of the polar grid. Even though the singularity can be avoided by partitioning each diameter into an even number of equally spaced lattice points (see Fig. 1), the presence of small denominators, i.e., $(1/r^4)\partial_{\phi\phi\phi\phi}$, at points close to the origin makes the resulting system quite ill conditioned and extremely sensitive to errors in the spatial derivatives. The algorithm presented in [11] utilizes distributed approximating functionals [13] and aims at approximating the flame front $u(r,\phi,t)$ and its spatial derivatives to high accuracy on and off the grid points, in order to mitigate the ill conditioning.

Even though great care was taken in [11] to develop an algorithm that captures the spatial derivatives to high accuracy, it turns out that the algorithm is not well suited for *long-time* integration, especially of complex patterns, due to an instability caused by the treatment of the nonlinear terms in the expression for the *temporal derivative*.

In Sec. III we quickly review distributed approximating functionals. Then, in Sec. IV A we describe the weakness in the temporal approximation scheme used in [11], and in Sec. IV B we propose an alternative treatment of the temporal derivative. Finally, in Sec. V we showcase some numerical results obtained using this scheme.

III. DISTRIBUTED APPROXIMATING FUNCTIONALS

Distributed approximating functionals (DAFs) have been carefully analyzed [13–16] and have successfully been applied to a wide range of applications, e.g., atom-atom potentials [17], rovibrational states of H_3^+ [18], path integrals for quantal many-body dynamics [19], and the Fokker-Planck equation [20]. Given its wide acceptance, and range of applicability, we only briefly review the DAF concept, and refer the reader to the literature.

DAF based schemes are generated by expressing spatial derivatives in the weak form (2),

$$f^{(k)}(x) = (-1)^k \int_{-\infty}^{\infty} \delta^{(k)}(x) f(x) dx \approx (-1)^k \int_{-\infty}^{\infty} \delta_{\mathrm{DAF}}{}^{(k)}(x) f(x) dx, \tag{2}$$

approximating the δ-function and its derivatives $\delta^{(k)}$, and then applying a quadrature rule to the integration, thus yielding $f_{\mathrm{DAF}}^{(k)}(x)$. Robust DAF schemes can be built by approximations to the δ function generated by multiplication of a Gaussian by a finite sum of orthogonal polynomials, e.g., Hermite polynomials [17],

$$\delta_{\mathrm{DAF}}(x) = \frac{1}{\sqrt{2\pi}\sigma} e^{-x^2/2\sigma^2} \sum_{n=0}^{M/2} \frac{1}{(-4)^n} \frac{1}{n!} H_{2n}\left(\frac{x}{\sqrt{2}\sigma}\right), \tag{3}$$

$$(-1)^k \delta_{\mathrm{DAF}}(x)^{(k)} = \frac{1}{\sqrt{2^k}\pi\sigma^{k+1}} e^{-x^2/2\sigma^2} \times \sum_{n=0}^{M/2} \frac{1}{(-4)^n} \frac{1}{n!} H_{2n+k}\left(\frac{x}{\sqrt{2}\sigma}\right) \tag{4}$$

where M is the order of approximation, and σ is an appropriate decay rate for the exponential. DAFs are particularly well suited for approximating spatial derivatives on nonuniform grids since the error bound for the approximation is uniform over the entire domain, even off the node points. In our application the quadrature points for the integration are given by the regular grid (Fig. 1).

IV. TIME INTEGRATION OF THE KURAMOTO-SIVANSHINSKY EQUATIONS

Given the DAF representation of the spatial derivatives, we now turn our attention to the time integration of the Kuramoto-Sivanshinsky equation. In order to simplify the notation we let $\vec{x}=(r,\phi)$ and let $F(\vec{x},t,u(t))$ represent the right-hand side of the Kuramoto-Sivanshinsky equation (1), where for convenience we suppress the dependence on $\vec{x}$. We have

$$u_t(t) = F(\vec{x},t,u(t)), \tag{5}$$

where $F(\vec{x},t,u(t))$ decomposes into a linear and nonlinear operator on $u(t)$, i.e.,

$$F_{\mathrm{lin}}(\vec{x},t,u(t)) = -u_{rrrr} - \frac{1}{r^4}u_{\phi\phi\phi\phi} - \frac{2}{r^2}u_{rr\phi\phi} - \frac{2}{r}u_{rrr} + \frac{2}{r^3}u_{r\phi\phi} - \left(2-\frac{1}{r^2}\right)u_{rr} - \left(\frac{4}{r^4}+\frac{2}{r^2}\right)u_{\phi\phi} - \left(\frac{1}{r^3}+\frac{2}{r}\right)u_r + \eta_1 u,$$

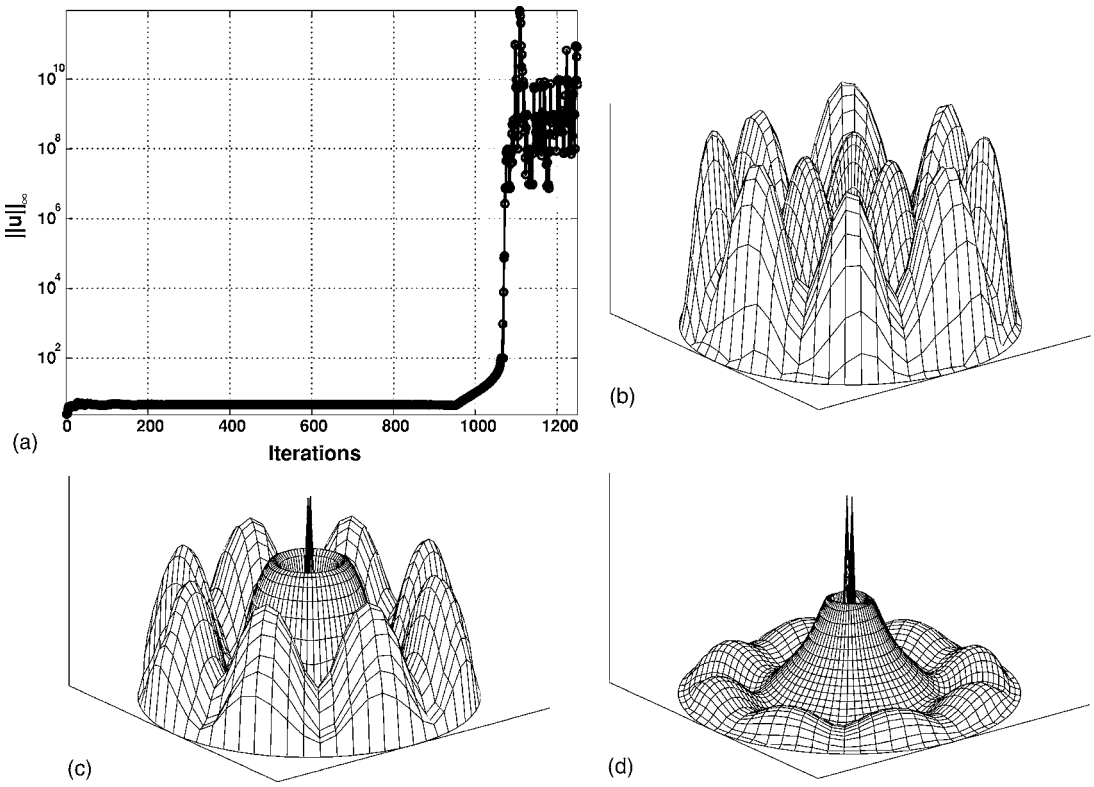

FIG. 2. Simulation using the linearization from [11]. (a) shows the max-norm of the solution, $\|u(\cdot)\|_\infty$, as a function of the number of iterations; it stays relatively constant ≈ 5 for 900 iterations, and then blows up by several orders of magnitude with a peak at $\approx 10^{12}$. (b) shows a snapshot of the pattern, in which the interior ring rotates clockwise, and the exterior ring rotates counterclockwise, at iteration 900. (c) shows the solution at iteration 975, just as the error in the center of the domain starts to dominate the behavior. (d) shows the complete dominance of the error at iteration 1050. The simulation parameters are $\eta_1 = 0.32$, $\eta_2 = 1$, $\eta_3 = 0.017$, and $R = 12.0$.

$$F_{\mathrm{nl}}(\vec{x},t,u(t)) = -\eta_2\left(u_r^2 + \frac{1}{r^2}u_\phi^2\right) - \eta_3 u^3. \tag{6}$$

We note that with the DAF representation every spatial derivative can be expressed as a sum over the domain, with appropriate weights, e.g.,

$$u_{rr}(r,\phi) = \sum_{r_i=1,\phi_i=1}^{N_r,N_\phi} w_{\mathrm{DAF}}^{rr}(r_i - r, \phi_i - \phi)u(r_i,\phi_i), \tag{7}$$

where $\{r_1, r_2, \ldots, r_{N_r}\}$ and $\{\phi_1, \phi_2, \ldots, \phi_{N_\phi}\}$ represent the discretization of the grid in the radial and azimuthal coordinates, respectively. The weight coefficients for each derivative depend only on the order of approximation M and the decay parameter σ in the DAF description, as well as the grid geometry, and can therefore be computed once and for all. We now focus our attention on the treatment of the nonlinear term $F_{\mathrm{nl}}(\vec{x},t,u(t))$.

A. The Zhang *et al.* approach

In [11] the proposed DAF based time-integration scheme for the Kuramoto-Sivanshinsky model is expressed in the form

$$\frac{u(t+h)-u(t)}{h} = F\left(\vec{x}, t+\frac{h}{2}, \frac{u(t+h)+u(t)}{2}\right), \tag{8}$$

i.e., the right-hand side is evaluated at the central time $t+h/2$, in order to achieve second-order accuracy in the time integration. The nonlinear terms $F_{\mathrm{nl}}(\vec{x},t,u(t))$ give the following contributions to the right-hand side of Eq. (8):

$$\left(\frac{u(t+h)+u(t)}{2}\right)^3 = \frac{1}{8}[u(t+h)^3 + 3u(t+h)^2u(t) + 3u(t+h)u(t)^2 + u(t)^3], \tag{9}$$

$$\left(\frac{u_s(t+h)+u_s(t)}{2}\right)^2 = \frac{1}{4}[u_s(t+h)^2 + 2u_s(t+h)u_s(t) + u_s(t)^2], \quad s = \{r,\phi\}. \tag{10}$$

In order to get a linear system in $u(t+h)$ and its variables, the following linearization is used:

$$\left(\frac{v(t+h)+v(t)}{2}\right)^n \approx \left(1-\frac{n}{2}\right)v(t)^n + \frac{n}{2}v(t)^{n-1}v(t+h), \tag{11}$$

yielding

```
A = δG⃗_lin(u⃗(x⃗,0))
// Time-loop, t = k·h
for( k=0 ; k≤kmax; k++ ) {
  // Newton iteration
  n=0,  v⃗^0(x⃗) = u⃗(x⃗, k·h)
  do {
    B = δG⃗_nl(v⃗^n(x⃗))
    δv⃗ = BiCGSTAB( A, A+B, G⃗(v⃗^n(x⃗)) )
    v⃗^{n+1}(x⃗) = v⃗^n(x⃗) − δv⃗
    n = n + 1
  } while( ||G⃗(v⃗^n(x⃗))|| ≤ tol·||G⃗(v⃗^0(x⃗))|| )
  u⃗(x⃗,(k+1)h) = v⃗^n(x⃗)
} // end-for
```

FIG. 3. The algorithmic core of the integration scheme. The call to BiCGSTAB solves $(A+B)\delta\vec{v}=G(\vec{v}(\vec{x},n))$ iteratively, using the preconditioner A.

$$\left(\frac{u(t+h)+u(t)}{2}\right)^3 \approx \frac{-u(t)^3+3u(t)^2u(t+h)}{2}, \tag{12}$$

$$\left(\frac{u_s(t+h)+u_s(t)}{2}\right)^2 \approx u_s(t)u_s(t+h), \tag{13}$$

where in Eq. (13) $s=\{r,\phi\}$. The resulting scheme is unstable for integration over long periods of time, especially when highly complex patterns are formed. In particular, the errors in the center of the domain grow exponentially and dominate the solution, generically within less than a thousand iterations even for relatively simple patterns, one illustration is shown in Fig. 2.

An explanation as to why this exponential error growth should occur follows from careful analysis of the approximation errors introduced. Taylor-expanding Eq. (8) around $t+h/2$ shows that the errors due to the nonlinear terms on the right-hand side are, to leading order, of the form

$$-\eta_2\left(\frac{1}{4}u_su_{stt}-\frac{1}{4}u_{st}^2\right)h^2, \quad \text{second order}, \tag{14}$$

$$-\eta_3\left(\frac{3}{8}u_{tt}u^2-\frac{3}{4}u_t^2u\right)h^2, \quad \text{third order}. \tag{15}$$

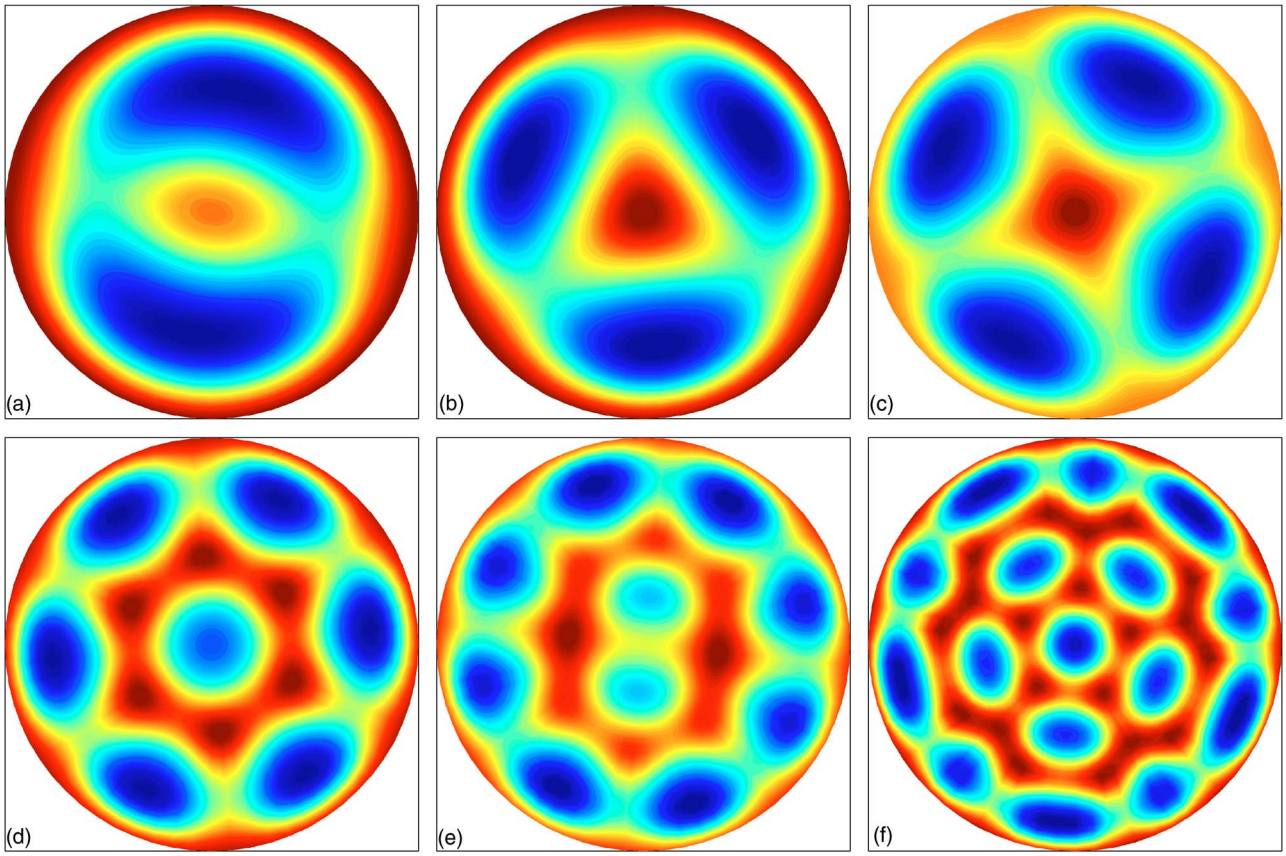

FIG. 4. (Color online) Some of the static patterns observed using the Kuramoto-Sivanshinsky integration scheme. (a), two-cell pattern, $R=5.0$; (b), three-cell pattern, $R=6.0$; (c), four-cell pattern, $R=8.0$; (d), 6/1-cell pattern, $R=10.0$; (e), 8/2-cell pattern, $R=12.0$; (f), 10/5/1-cell pattern, $R=14.5$. Common simulation parameters: $(\eta_1,\eta_2,\eta_3)=(0.32,1.00,0.017)$.

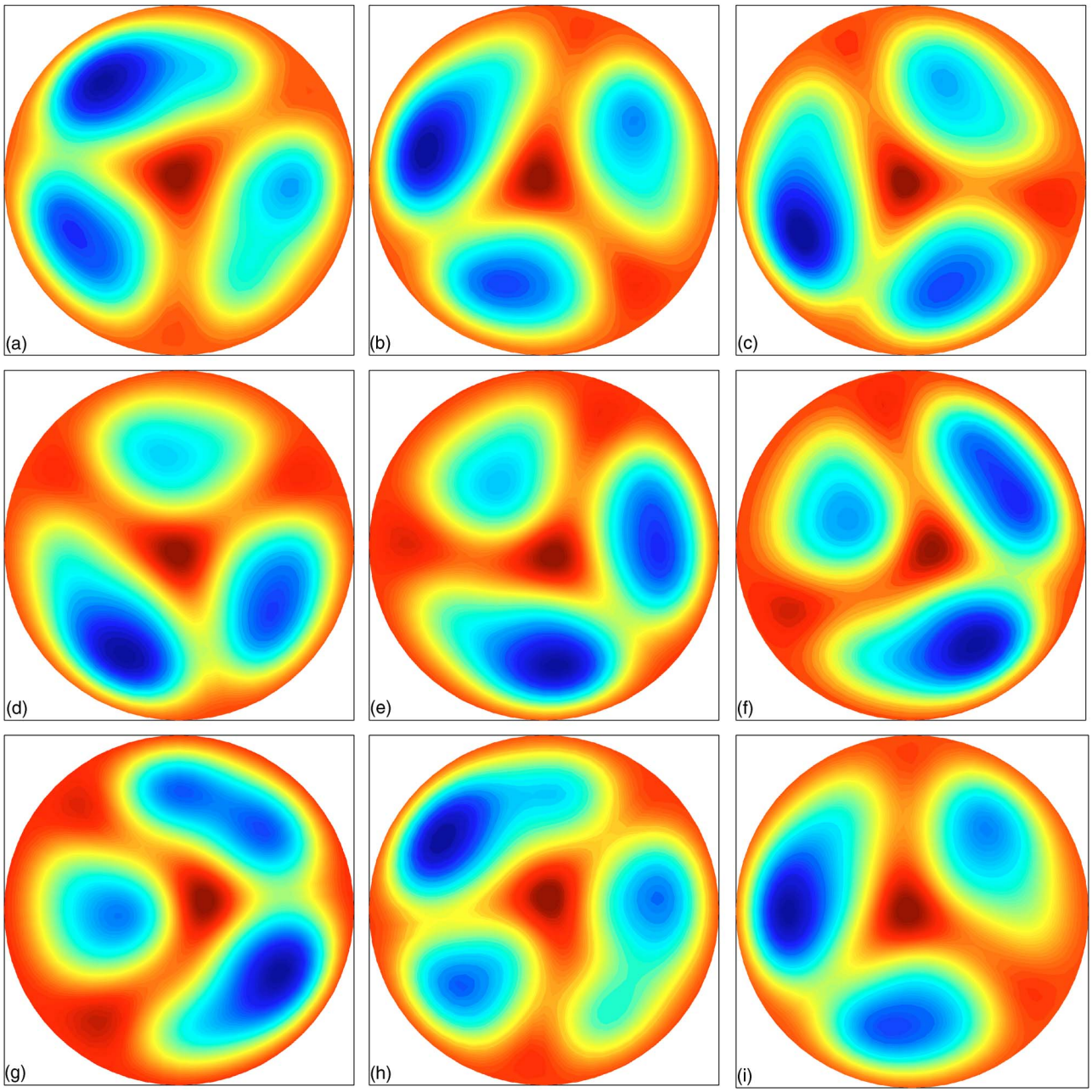

FIG. 5. (Color online) Snapshots of a three-cell hopping state from a simulation of Eq. (1). The pattern is shown at times $t \in \{0,15,30,45,60,75,90,105,120,135\}$; time evolves from left to right and top to bottom in the panels. The simulation parameter values are $(\eta_1, \eta_2, \eta_3; R) = (0.32, 1.00, 0.017; 7.7475)$. In this sequence we see how the frontrunner of the two-cell formation bridges the gap to the solitary cell.

The second part of the second-order error, $+\eta_2 h^2 u_{st}^2/4$, is always positive and acts as a destabilizing factor. When we compare these errors with the ones introduced in the scheme proposed in the present paper [see Eqs. (17) and (18)], we will notice that the present scheme has a *stabilizing* factor of the same form. We note that the signs of the remaining three terms that comprise the approximation error are indeterminate and their effects cannot be interpreted as purely stabilizing or destabilizing.

B. The Crank-Nicolson based approach

We propose a time-integration algorithm based on the semi-implicit Crank-Nicolson [12] scheme. With $F(\vec{x}, t, u(t))$ as before, we write

$$\frac{u(t+h) - u(t)}{h} = \frac{F(x,t,u(t)) + F(x,t+h,u(t+h))}{2}. \quad (16)$$

We remark that the Crank-Nicolson scheme is only used for the time component; the DAF representation is maintained in

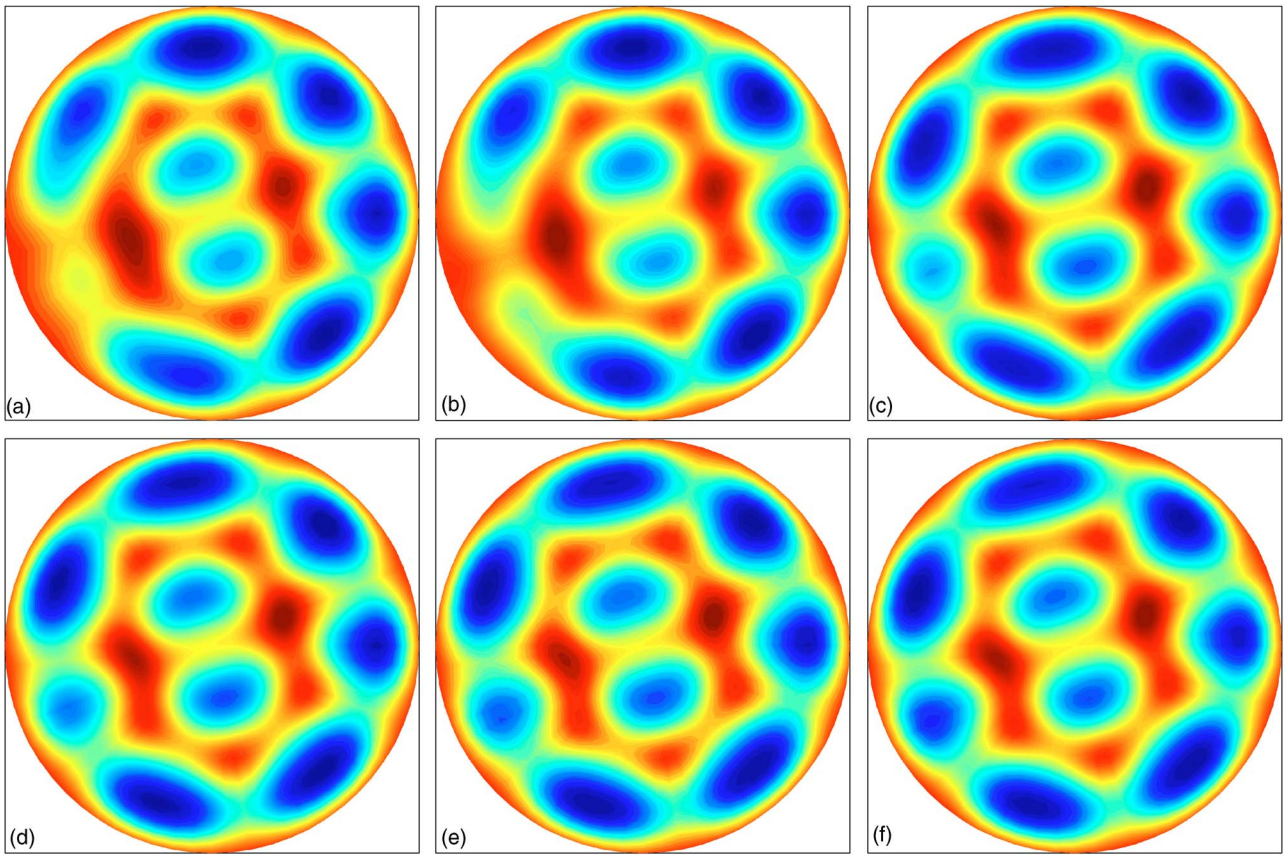

FIG. 6. (Color online) Snapshots of the first stage of the evolution of the 8/2-cell pattern, time evolves from left to right and top to bottom in the panels. Here, the number of cells in the outer ring fluctuates between 7 and 8, as illustrated in the six panels. The location of the splitting and merging of the outer cells changes over time. This phase persists for times up to $t=3400$.

order to generate high-accuracy approximations to the spatial derivatives. The Crank-Nicolson scheme provides unconditional stability [21]. Taylor-expanding Eq. (16) around $t+h/2$ shows that the approximation errors due to the nonlinear terms are, to leading order,

$$-\eta_2\left(\frac{1}{4}u_s u_{stt}+\frac{1}{4}u_{st}^2\right)h^2, \quad \text{second order}, \tag{17}$$

$$-\eta_3\left(\frac{3}{8}u_{tt}u^2+\frac{3}{4}u_t^2 u\right)h^2, \quad \text{third order}. \tag{18}$$

These error terms are very similar to the ones derived for the previous approach, in Eqs. (14) and (15). The signs of two of the contributing terms have changed, and here the second part of the second-order term now provides a stabilizing factor.

We now focus our attention on using the complete nonlinear system (16) in order to devise a numerical scheme. With the spatial derivatives represented by the DAF approximations (7) we get a nonlinear system of equations (19)

$$\vec{G}(\vec{u}(\vec{x},t+h))=0, \tag{19}$$

where

$$\vec{G}(\vec{u}(\vec{x},t+h))=\vec{G}_{\text{lin}}(\vec{u}(\vec{x},t+h))+\vec{G}_{\text{nl}}(\vec{u}(\vec{x},t+h)), \tag{20}$$

with

$$\vec{G}_{\text{lin}}(\vec{u}(t+h))=\left(\frac{\vec{u}(t+h)}{2}-\frac{\vec{u}(t)}{2}\right)-\left(\frac{F_{\text{lin}}(x,t+h,\vec{u}(t+h))}{2}+\frac{F_{\text{lin}}(x,t,\vec{u}(t))}{2}\right), \tag{21}$$

$$\vec{G}_{\text{nl}}(\vec{u}(t+h))=-\left(\frac{F_{\text{nl}}(x,t+h,\vec{u}(t+h))}{2}+\frac{F_{\text{nl}}(x,t,\vec{u}(t))}{2}\right), \tag{22}$$

in which $\vec{u}(\vec{x},t+h)$ are the unknowns, and $\vec{u}(\vec{x},t)$ are known. We solve this using an iterative Newton based method

$$\vec{u}^{n+1}(\vec{x},t+h)=\vec{u}^{n}(\vec{x},t+h)-[\delta\vec{G}(\vec{u}^{n}(\vec{x},t+h))]^{-1}\cdot\vec{G}(\vec{u}^{n}(\vec{x},t+h)), \tag{23}$$

$$\vec{u}^{0}(\vec{x},t+h)=\vec{u}(\vec{x},t), \tag{24}$$

where $\delta\vec{G}=\nabla_u\vec{G}(\vec{u}^n(\vec{x},t+h)$ is the Jacobian. The Newton iteration is repeated until the residual is reduced sufficiently, e.g.,

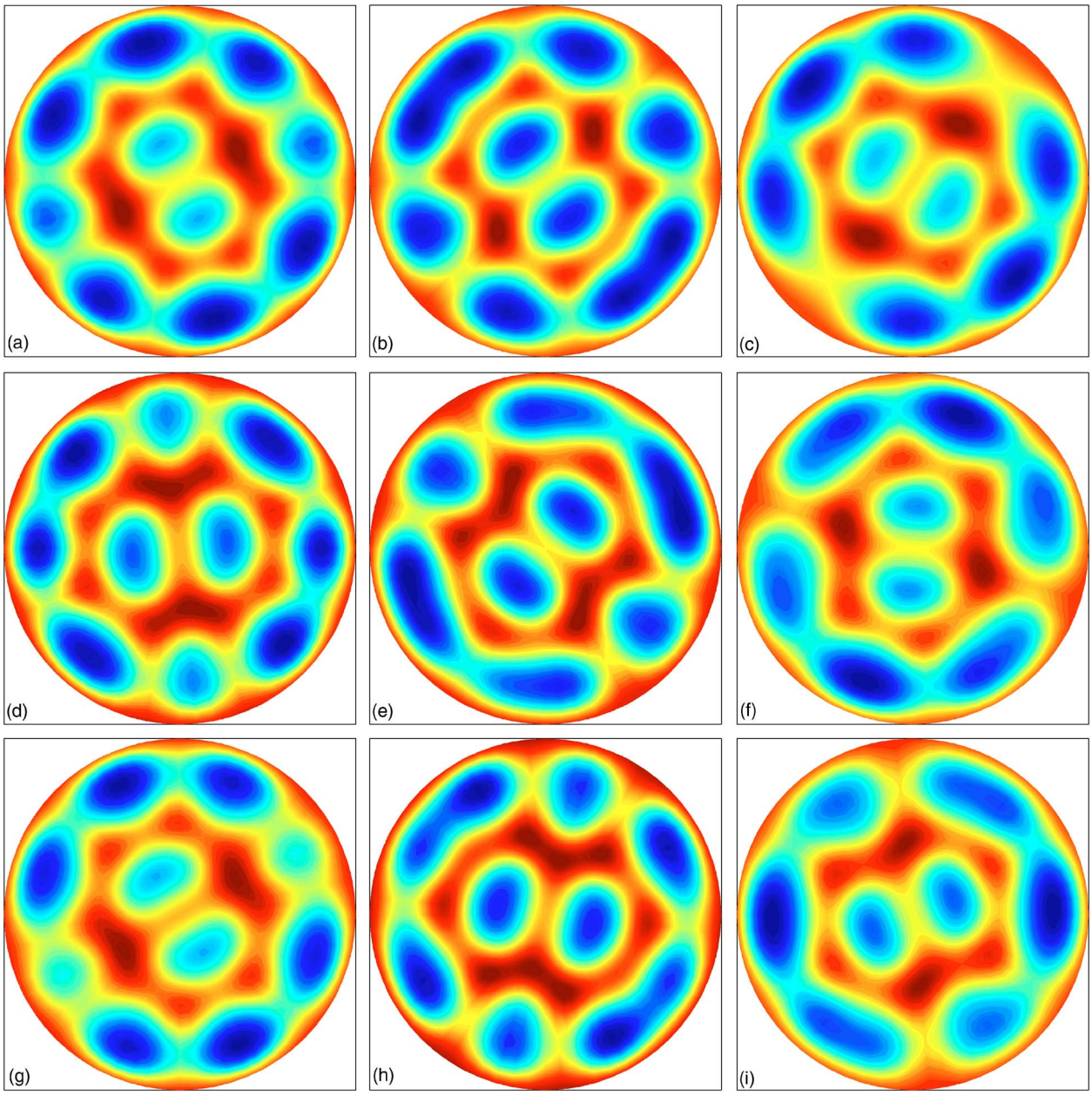

FIG. 7. (Color online) Snapshots of the second stage of evolution for the 8/2-cell pattern; time evolves from left to right and top to bottom in the panels. In this stage the number of cells in the outer ring fluctuates between 6 and 8, and the two cells in the inner ring rotate counterclockwise while fluctuating in magnitude. This stage persists for times $t \in [3400, 5500]$, after which it settles into the stationary 8/2-cell pattern shown in the Fig. 4(e).

$$\|\vec{G}(\vec{u}^{n+1}(\vec{x},t+h))\| \leqslant \mathcal{T}\|\vec{G}(\vec{u}^{0}(\vec{x},t+h))\|, \tag{25}$$

in our implementation $\mathcal{T}=10^{-6}$, and the number of required Newton iterations is about 25. In each step of the Newton iteration we have to solve the linear system

$$[\delta\vec{G}(\vec{u}^{n}(\vec{x},t+h))]\delta\vec{u} = \vec{G}(\vec{u}^{n}(\vec{x},t+h)). \tag{26}$$

In our computational setup, where the grid is subdivided into $N_r=32$ radial points, and $N_\phi=64$ azimuthal points, this leads to a nearly dense 2048×2048 system. We solve this using the preconditioned biconjugate gradient stabilized method [Bi-CGSTAB(M)] [22], where a good preconditioner can be extracted by noticing that the decomposition into linear and nonlinear contributions described in Eqs. (20)–(22) of the system is transitive to the Jacobian, and we have

$$\delta\vec{G}(\vec{u}(\vec{x},t+h)) = \delta\vec{G}_{\text{lin}}(\vec{u}(\vec{x},t+h)) + \delta\vec{G}_{\text{nl}}(\vec{u}(\vec{x},t+h)), \tag{27}$$

where $\delta\vec{G}_{\text{lin}}(\vec{u}(\vec{x},t+h))$ is constituted from contributions from DAF derivative coefficients (7) and therefore does not depend on $\vec{u}(\vec{x},t+h)$. We let the linear part define our preconditioner, i.e., $M=\delta\vec{G}_{\text{lin}}(\vec{u}(\vec{x},t+h))$. The preconditioner M is used with a fast solver for the linear system $M\vec{v}=\vec{w}$, based

e.g., on the LU, or QR decomposition of M, which can be computed once for the Bi-CGSTAB(M) algorithm. We summarize the algorithm in Fig. 3.

V. NUMERICAL RESULTS

We have implemented the algorithm described in Sec. IV B, and have validated the results by several observations of stationary and dynamic patterns that had only been previously observed in physical experiments. In Fig. 4 we show six different static patterns; the parameters $(\eta_1, \eta_2, \eta_3) = (0.32, 1.00, 0.017)$ are being held constant and as the radius R of the burner increases, the pattern goes through a series of symmetry-breaking bifurcations increasing the complexity of the pattern.

For dynamic patterns, we can generate extremely long-time-series data which allows us to capture many rotations in rotating or hopping patterns. A careful study of a numerically simulated three-cell hopping state is being reported in [23]. A hopping state (illustrated in Fig. 5) is a modulated nonrigid rotation in which one of the cells "bridges the gap" to the cell in front of it and thus leaves a gap to the cell behind it; the "gapped" cell eventually bridges the newly created gap, etc.

The hopping state is not the only unusual pattern observed. The 8/2-cell pattern in Fig. 4(e) is stationary; however, the route to this stationary pattern is interesting. From an arbitrarily chosen initial state, the pattern goes through a sequence of behaviors. First, there is a quick transition in which the two rings of cells are formed; then for an extended period of time (until approximately $t = 3400$), we observe the first persistent dynamic state, in which the two interior cells are stationary while the number of cells in the outer ring fluctuates between 7 and 8 (see Fig. 6). In the time interval $3400 < t < 5500$ we observe a second persistent dynamic state, in which the number of cells in the outer ring fluctuates between 6 and 8 while the two interior cells rotate counterclockwise while fluctuating in magnitude (see Fig. 7).

VI. CONCLUSION

We have devised a numerical integration scheme for the Kuramoto-Sivanshinsky equation in a circular domain. By combining treatment of the representation of the spatial derivatives using distributed approximating functionals with a linearly unconditionally A-stable Crank-Nicolson integration in time our scheme achieves high accuracy and extreme robustness.

The solutions to the nonlinear systems resulting from the Crank-Nicolson scheme are found using a Newton iteration where the resulting linear systems are solved using the preconditioned biconjugate gradient stabilized algorithm [Bi-CGSTAB(M)].

We have demonstrated the ability of our scheme to successfully simulate a significant number of stationary and nonstationary solutions to the Kuramoto-Sivanshinsky equation, over extended periods of time. This allows us to identify and classify the evolution of unusual patterns. In a separate paper [23] we have performed a detailed principal mode study of the first such pattern, the three-cell hopping state.

Finally we note that even though we have solved a very particular problem, the approach is quite generic. The framework provided by the distributed approximating functionals for generating high-order accurate numerical approximations of the spatial derivatives is applicable to any problem, expressed on a regular or nonregular grid. Further, basing the time integration on a Crank-Nicolson scheme in order to generate a scheme with highly desirable stability properties is a time-tested approach.

APPENDIX: A-STABILITY OF THE CRANK-NICOLSON SCHEME

Linear von Neumann analysis

Von Neumann analysis is an application of Fourier analysis devised to study the stability properties of finite difference schemes. To linear order it applies to systems of equations

$$\frac{\partial}{\partial t}\hat{\mathbf{y}} = L\hat{\mathbf{y}}, \tag{A1}$$

where L is a matrix capturing the finite difference (of DAF representation) of spatial derivatives of $\hat{\mathbf{y}}$. After an appropriate change of basis, using the unitary Schur factorization $QTQ^* = L$, we can express Eq. (A1) in the transformed coordinate $\vec{y} = Q^*\hat{\mathbf{y}}$,

$$\frac{\partial}{\partial t}\vec{y} = T\vec{y} \tag{A2}$$

where T is upper triangular, with $T_{ii} = \lambda_i$. We can now limit our study to scalar equations

$$\frac{\partial}{\partial t}y = \lambda y \tag{A3}$$

and note that if $\mathrm{Re}(\lambda) < 0$, then $\lim_{t\to\infty} y(t) = 0$. Now, we integrate Eq. (A3) in time using the Crank-Nicolson scheme

$$\frac{y^{(n+1)} - y^{(n)}}{dt} = \frac{\lambda}{2}(y^{(n+1)} + y^{(n)}), \tag{A4}$$

which, with $\hat{h} = \lambda dt$, gives

$$y^{(n+1)} = \underbrace{\left(\frac{1+\hat{h}/2}{1-\hat{h}/2}\right)}_{g_{\mathrm{CN}}(\hat{h})} y^{(n)}. \tag{A5}$$

Here $g_{\mathrm{CN}}(\hat{h})$ is the amplification factor for the Crank-Nicolson scheme. The region of *absolute stability* for an integration scheme is defined in terms of the amplification factor

$$R_A = \{\hat{h} \in C: |g(\hat{h})| < 1\}, \tag{A6}$$

i.e., all the values of $\hat{h}$ for which $\lim_{n\to\infty} y^{(n)} = 0$. If $R_A \supseteq \{\hat{h}: \mathrm{Re}(\hat{h}) < 0\}$, then the method is said to be *A-stable*. From Eq. (A5) it immediately follows that $R_A^{\mathrm{CN}} \equiv \{\hat{h} \in \mathbb{C}: |g(\hat{h})| < 1\}$, so that the Crank-Nicolson integration is unconditionally *A*-stable, independent of the time step *dt*.

[1] Q. Ouyang and H. L. Swinney, Nature (London) **352**, 610 (1991).
[2] M. S. Heutmaker and J. P. Gollub, Phys. Rev. A **35**, 242 (1987).
[3] M. Gorman, M. el Hamdi, and K. Robbins, Combust. Sci. Technol. **98**, 47 (1994).
[4] M. Gorman, M. el Hamdi, and K. Robbins, Combust. Sci. Technol. **98**, 79 (1994).
[5] M. Gorman, M. el Hamdi, and K. Robbins, Combust. Sci. Technol. **98**, 71 (1994).
[6] M. Gorman, M. el Hamdi, and K. Robbins, Combust. Sci. Technol. **98**, 25 (1994).
[7] Y. Kuramoto, Suppl. Prog. Theor. Phys. **64**, 346 (1978).
[8] G. I. Sivashinsky, Combust. Sci. Technol. **15**, 137 (1977).
[9] G. I. Sivashinsky, Acta Astronaut. **4**, 1177 (1977).
[10] M. Gorman, M. el-Hamdi, B. Pearson, and K. A. Robbins, Phys. Rev. Lett. **76**, 228 (1996).
[11] D. S. Zhang, G. W. Wei, D. J. Kouri, D. K. Hoffman, M. Gorman, A. Palacios, and G. H. Gunaratne, Phys. Rev. E **60**, 3353 (1999).
[12] J. Crank and P. Nicolson, Proc. Cambridge Philos. Soc. **43**, 50 (1947); republished in Adv. Comput. Math. **6**, 207 (1997), John Crank 80th birthday special issue.
[13] D. K. Hoffman, T. L. Marchioro II, M. Arnold, Y. Huang, W. Zhu, and D. J. Kouri, J. Math. Chem. **20**, 117 (1996).
[14] D. K. Hoffman, M. Arnold, and D. J. Kouri, J. Phys. Chem. **96**, 6539 (1992).
[15] D. K. Hoffman and D. J. Kouri, J. Phys. Chem. **96**, 1179 (1992).
[16] D. K. Hoffman, G. W. Wei, D. S. Zhang, and D. J. Kouri, Phys. Rev. E **57**, 6152 (1998).
[17] A. M. Frishman, D. K. Hoffman, R. J. Rakauskas, and D. J. Kouri, Chem. Phys. Lett. **151**, 62 (1996).
[18] S. S. Iyengar, G. A. Parker, D. J. Kouri, and D. K. Hoffman, J. Chem. Phys. **110**, 10283 (1999).
[19] D. J. Kouri, W. Zhu, X. Ma, B. M. Pettitt, and D. K. Hoffman, J. Phys. Chem. **96**, 9622 (1992).
[20] D. S. Zhang, G. W. Wei, D. J. Kouri, and D. K. Hoffman, J. Chem. Phys. **106**, 5216 (1997).
[21] J. C. Strikwerda, *Finite Difference Schemes and Partial Differential Equations*, 2nd ed. (SIAM, Philadelphia, PA, 2004).
[22] R. Barrett, M. Berry, T. F. Chan, J. Demmel, J. Donato, J. Dongarra, V. Eijkhout, R. Pozo, C. Romine, and H. V. der Vorst, *Templates for the Solution of Linear Systems: Building Blocks for Iterative Methods*, 2nd ed. (SIAM, Philadelphia, PA, 1994).
[23] P. Blomgren, S. Gasner, and A. Palacios, Chaos **15**, 013706 (2005).